JOURNAL OF MATERIALS SCIENCE LETTERS 24 (1989) 2151–2164

Lifetime statistics for single graphite fibres in creep rupture

D. S. FARQUHAR, F. M. MUTRELLE, S. L. PHOENIX
Sibley School of Mechanical and Aerospace Engineering, Upson Hall, Cornell University, Ithaca, New York 14853, USA

R. L. SMITH
Department of Mathematics, University of Surrey, Guildford, Surrey GU2 5XH, UK

Experimental results are presented for the lifetime in creep rupture of single graphite fibres. The fibres were extracted from unsized, Hercules IM6 tows and were tested at a gauge length of 5 cm under standard ambient conditions (21°C, 50% r.h.). The results were analysed using a theoretical model which embodies Weibull distributions for both strength and lifetime, and a power-law relationship for lifetime against stress level. Using maximum likelihood techniques, the Weibull shape parameter values for strength and lifetime were found to be about 4.6 and 0.015, respectively, and the power-law exponent was about 300, but could be as low as 250. As expected, this exponent was close in value to the ratio of the respective Weibull shape parameter values. Using the Kaplan–Meier estimator for censored data, the goodness of fit of the model to the data was found to be excellent.

1. Introduction

For over two decades research has been conducted to develop lightweight, filamentary composite structures which can reliably sustain high tensile loads for long time periods. An important material for such applications has been graphite or carbon fibres in an epoxy matrix, and typical structures include filament-wound pressure vessels, composite flywheels, gas centrifuge cylinders, rocket motor casings and structural beams. These structures are often used in critical aerospace and defence applications where failures can have disastrous consequences.

In the above applications the composite is subject to the random and catastrophic phenomenon of creep rupture (variously called stress rupture, static fatigue, creep fatigue and stress-life failure). To establish the creep-rupture properties for design purposes, various laboratories have resorted to experimentally testing large numbers of epoxy-impregnated strands, since testing a sufficient number of full-scale structures is prohibitively expensive. The hope has been that simple scaling laws could be applied to forecast structural life from strand results. For example, tests have been performed on Union Carbide Thornel 50 graphite–epoxy strands [1], Torayca T300 carbon–epoxy strands [2], Hercules AS4 graphite–epoxy strands [3], and Hercules IM6 graphite–epoxy strands and NOL rings [4]. Also work was recently carried out at Cornell University on model composites consisting of seven Hercules IM6 graphite fibres in an epoxy matrix [5].

The results of these strand experiments show large statistical variations in lifetime for ostensibly identical specimens, but more important perhaps is the fact that the sensitivity of median lifetime to stress level varies widely depending on the composite material system. Using the usual power law to relate median lifetime to stress level, power-law exponents ranging from 60 to 120 can be inferred from the data. In fact, similar material systems (differing say by lot number) have been found to vary by 40% in this key parameter. Unfortunately, separate testing has not been carried out on the individual fibres and the epoxy matrix so that it is not possible to investigate the source of the above variation in the strands. This variation is important because it introduces considerable uncertainty and risk in forecasting structural life and reliability.

Failure in these composites is generally a complex statistical process involving scattered failure of fibres at flaw sites, overloading of neighbouring fibres by way of stress transfer through the matrix, and the growth of clusters of adjacent fibre breaks to a critical unstable size. In creep rupture under a steady load, failure is further enhanced by a combination of thermally activated flaw growth and failure in the fibres, viscoelastic creep in the matrix near breaks, and progressive debonding at the fibre–matrix interface. The latter two mechanisms result in a widening pattern of overloading on fibres next to existing breaks causing additional breaks. The result is sequences of adjacent fibre breaks which grow in time and form small clusters or "cracks", one of which ultimately becomes unstable and triggers failure of the composite.

It is often assumed that the graphite fibres themselves are virtually immune to creep rupture, implying that thermally activated flaw growth may be neglected as compared to both matrix creep and interface failure effects in the composite. Phoenix *et al.* [5] have

0022–2461/89 $03.00 + .12

developed a model for creep rupture of such composites based on this assumption. One reason why this assumption has not been tested is the huge inherent variability which occurs in fibre lifetime. This variability necessitates testing large numbers of individual fibres, and using sophisticated statistical modelling and analysis techniques to interpret the results. Typical observations on testing a few graphite fibre specimens are that they fail on loading or seem to last indefinitely. These difficulties have, in fact, discouraged the generation of creep-rupture data on all types of high-strength fibres.

The main purpose of this paper is to report on creep-rupture tests on single graphite fibres and to determine statistical and power-law parameters for a certain model of fibre lifetime. The model has Weibull features for both strength and lifetime, and power-law behaviour in relating lifetime in creep rupture to stress level. First the use and justification of the fibre model is discussed and the experimental techniques are described. Then the results of the various strength and lifetime experiments are presented and analysed using maximum likelihood techniques. Analyses are presented for the individual sets of data first, and then for all the data at once using a full likelihood analysis. Lastly, we study the goodness of fit of the model to the data using the Kaplan–Meier estimator for censored data, and find an excellent fit.

2. Statistical model for failure of single fibres

2.1. General formulation of the model

Single fibres are subject to the creep-rupture failure process. Under a constant tensile stress, a single fibre (e.g. graphite, aramid or glass) though surviving at first, may fail after many hours. The failure originates at the atomic level. When sufficient thermal energy exists in a molecule to overcome certain local energy barriers, the molecule may slip relative to other molecules or rupture at one of its atomic bonds. As molecules slip or rupture, neighbouring molecules become overloaded and their failure rates are increased. Such molecular failures give rise to growing microcracks which eventually break the fibre. Moreover, the statistical variation in fibre strength and lifetime is governed both by random molecular failure and by randomly distributed structural imperfections or flaws.

The parametric form of the model was originally proposed by Coleman [6] on phenomenological grounds, and was justified theoretically by Phoenix and co-workers [7–9]. According to the model, the distribution function for the failure time t_F of a single fibre, loaded under the non-negative stress history $\sigma(t)$, $t \geqslant 0$ is a functional of the form

$$F(t; \sigma) = 1 - \exp\left[-\Psi\left\{\int_0^t \kappa[\sigma(u)]\mathrm{d}u\right\}\right] \qquad t \geqslant 0 \tag{1}$$

where $\kappa(x)$, $x \geqslant 0$ is called the breakdown rule, and $\Psi(x)$ is called the shape function. To impart the commonly observed Weibull behaviour to a fibre, a Weibull shape function is taken whereby

$$\Psi(x) = \alpha x^{\beta} \tag{2}$$

where α and β are positive constants. In keeping with the usual size effect, α is proportional to fibre length so that $\alpha = \alpha_0 l/l_0$, where l is the fibre length and α_0 is associated with the unit length l_0. (Length is not varied in the current experiments as it was by Phoenix *et al.* [5].) The breakdown rule κ is taken as the *power law breakdown rule*,

$$\kappa(x) = \gamma x^{\varrho} \tag{3}$$

where γ and ϱ are positive constants. Combining Equations 1, 2 and 3 the fibre model reduces to

$$F(t; \sigma) = 1 - \exp\left\{-\alpha\gamma^{\beta}\left[\int_0^t \sigma(u)^{\varrho}\mathrm{d}u\right]^{\beta}\right\} \qquad t \geqslant 0. \tag{4}$$

To justify the above model Phoenix [8] considered a lattice model for the failure of a single fibre wherein the molecules are aligned in parallel and fail randomly at bonds due to thermally activated chain scission. Adjacent to these failed bonds, neighbouring molecules are overloaded according to an elastic stress redistribution rule, thus increasing their thermally activated failure rate. Failure of the fibre results from the lateral growth of clusters of adjacent broken bonds, one of which develops into a catastrophic crack. Upon studying the typical shape of the function $U(\sigma)$ which is the required thermal energy for chain scission as a function of stress level σ (a Morse potential was used for illustration), Phoenix argued that the logarithmic function

$$U_1(\sigma) = -\tilde{U}_0 \ln(\sigma/\tilde{\sigma}_0) \tag{5}$$

where $\tilde{U}_0$ and $\tilde{\sigma}_0$ are adjustable parameters, provides a more accurate representation at high molecular stress levels than the widely used linear approximation $U_2(\sigma) = U_0 - \lambda\sigma$ where U_0 is the bond energy under zero stress (i.e. $U(0)$), and λ is the so-called activation volume (see also Phoenix and Tierney [7]). He showed that Equation 5 leads directly to the power-law breakdown rule (Equation 3) where the parameters γ and ϱ are

$$\gamma = \tau_0^{-1}\tilde{\sigma}_0^{-\varrho} \tag{6}$$

and

$$\varrho = \tilde{U}_0/kT \tag{7}$$

where τ_0 is a period of bond vibration, T is the absolute temperature and k is Boltzmann's constant. For the Morse potential, $\tilde{U}_0$ was found to be about $0.40U_0$ and $\tilde{\sigma}_0$ was about $0.95\sigma_0$, where σ_0 is the peak bond force as calculated from the potential function. Furthermore, Phoenix justified the integral form in Equation 1, and showed that the function $\Psi(x)$ is a complex function involving the elastic load-sharing constants and previous parameters but with approximately a power form as in Equation 2 with α proportional to the fibre volume. Phoenix and Kuo [9] showed that the exponent β can be much less than unity in the presence of randomly distributed initial defects such as chain ends. Later the experimental results are considered in this light.

2.2. Creep rupture under constant stress

For creep-rupture lifetime, consider the constant stress history

$$\boldsymbol{\sigma}_1(t) = \sigma \qquad t \geqslant 0 \tag{8}$$

where σ is a positive constant. The distribution function for lifetime (Equation 4) reduces to the Weibull distribution

$$F(t; \boldsymbol{\sigma}_1) = 1 - \exp\left[-(t/t_\sigma)^\beta\right] \tag{9}$$

where the scale parameter for lifetime is

$$t_\sigma = \sigma^{-\varrho}/(\alpha\gamma^\beta)^{1/\beta} \tag{10}$$

and the shape parameter is simply β.

2.3. Strength under linearly increasing stress

Next consider a linearly increasing stress history on a fibre such that

$$\boldsymbol{\sigma}_2(t) = Rt \qquad t \geqslant 0 \tag{11}$$

where the constant R is the loading rate. This is the stress history that is imposed during a tension test to measure the fibre's short-term strength Σ, which is equal to Rt_F where t_F is the failure time under this stress history. The distribution function for Σ is denoted as $F^*(\sigma)$ and is equivalent to $F(\sigma/R; \boldsymbol{\sigma}_2)$ which is easily calculated. The result is that the fibre strength follows the Weibull distribution,

$$F^*(\sigma) = 1 - \exp\left[-(\sigma/\sigma_R)^\eta\right] \tag{12}$$

where the shape parameter for strength is

$$\eta = \beta(\varrho + 1) \tag{13}$$

and the scale parameter for strength is

$$\sigma_R = (\alpha\gamma^\beta)^{-1/[\beta(\varrho+1)]}\,[R(\varrho + 1)]^{1/(\varrho+1)} \tag{14}$$

The sensitivity of fibre strength to loading rate is through the factor $R^{1/(\varrho+1)}$ and is very mild because ϱ is usually large.

2.4. Relation of scale parameters for strength and lifetime

Under the increasing stress history, (Equation 11) we let t_R be the time required for the stress to reach the Weibull scale parameter σ_R in value, that is,

$$t_R = \sigma_R/R \tag{15}$$

Upon combining Equations 10, 14, and 15 the lifetime scale parameter is

$$t_\sigma = \frac{(\sigma/\sigma_R)^{-\varrho} t_R}{(\varrho + 1)} \tag{16}$$

The Weibull scale parameter for lifetime under constant stress σ may be expressed simply as a power law in the stress ratio σ/σ_R, denoted by ϕ.

2.5. Actual experimental loading in creep rupture

In an actual creep-rupture experiment it is not possible to apply a constant load instantaneously. Thus, we consider a stress history with a loading phase, namely,

$$\boldsymbol{\sigma}_3(t) = \begin{cases} Rt & 0 \leqslant t < t_0 \\ \sigma & t_0 \leqslant t \end{cases} \tag{17}$$

where σ is the stress level for the test and R is the loading rate over the loading time $t_0 = \sigma/R$. From Equation 4 the distribution function for the failure time t_F is found to be

$$F(t; \boldsymbol{\sigma}_3) = \begin{cases} 1 - \exp\left[-\alpha\gamma^\beta R^{\varrho\beta}(\varrho + 1)^{-\beta} t^{\beta(\varrho+1)}\right] \\ \qquad\qquad 0 \leqslant t < t_0 \\ 1 - \exp\left\{-\alpha\gamma^\beta \sigma^{\varrho\beta}[t - t_0\varrho/(\varrho + 1)]^\beta\right\} \\ \qquad\qquad t_0 \leqslant t \end{cases} \tag{18}$$

It is useful to rewrite Equation 18 in terms of the respective Weibull shape and scale parameters for strength and lifetime derived earlier, and the stress ratio $\phi = \sigma/\sigma_R$. We first note the $t_0 = \phi t_R$, and using Equations 10 and 14 the distribution function becomes

$$F(t; \boldsymbol{\sigma}_3) = \begin{cases} 1 - \exp\left[-(t/t_R)^\eta\right] & 0 \leqslant t < \phi t_R \\ 1 - \exp\left\{-[(t - t_R^*)/t_\sigma]^\beta\right\} & \phi t_R \leqslant t \end{cases} \tag{19}$$

where

$$t_R^* = t_0\varrho/(\varrho + 1) = \phi t_R\varrho/(\varrho + 1) \tag{20}$$

being slightly less than t_0. Note that at longer times $t \gg t_0$, the second expression in Equation 19 reduces to Equation 9, the Weibull distribution function for lifetime under constant stress σ.

2.6. Failure rate for fibres

Because ϱ was expected to be very large (> 150) and β was expected to be very small (< 0.03), the fibre failure rate was considered in an effort to determine sample sizes and stress levels that would yield as much information as possible, that is, as many lifetime failures as possible during a reasonable time period. For this purpose it was useful to consider the lifetime density function

$$f(t; \boldsymbol{\sigma}) = \frac{\mathrm{d}}{\mathrm{d}t} F(t; \boldsymbol{\sigma}) \tag{21}$$

For the stress history $\boldsymbol{\sigma}_3(t)$, this density function is obtained from Equation 19 as

$$f(t; \boldsymbol{\sigma}_3) = \begin{cases} \eta t_R^{-1}(t/t_R)^{\eta-1} \exp\left[-(t/t_R)^\eta\right] & 0 \leqslant t < \phi t_R \\ \beta t_\sigma^{-1}[(t - t_R^*)/t_\sigma]^{\beta-1} \exp\left\{-[(t - t_R^*)/t_\sigma]^\beta\right\} & \\ \qquad\qquad \phi t_R \leqslant t \end{cases} \tag{22}$$

At longer times $t \gg t_0$ the above expression reduces to the standard Weibull density

$$f(t; \boldsymbol{\sigma}_3) \approx \beta t_\sigma^{-1}(t/t_\sigma)^{\beta-1} \exp\left[-(t/t_s)^\beta\right] \qquad \phi t_R \leqslant t \tag{23}$$

which is the density of Equation 9.

2.7. Optimal stress level for an experiment

In conducting a creep-rupture experiment, it is desirable to have the magnitude of the lifetime density

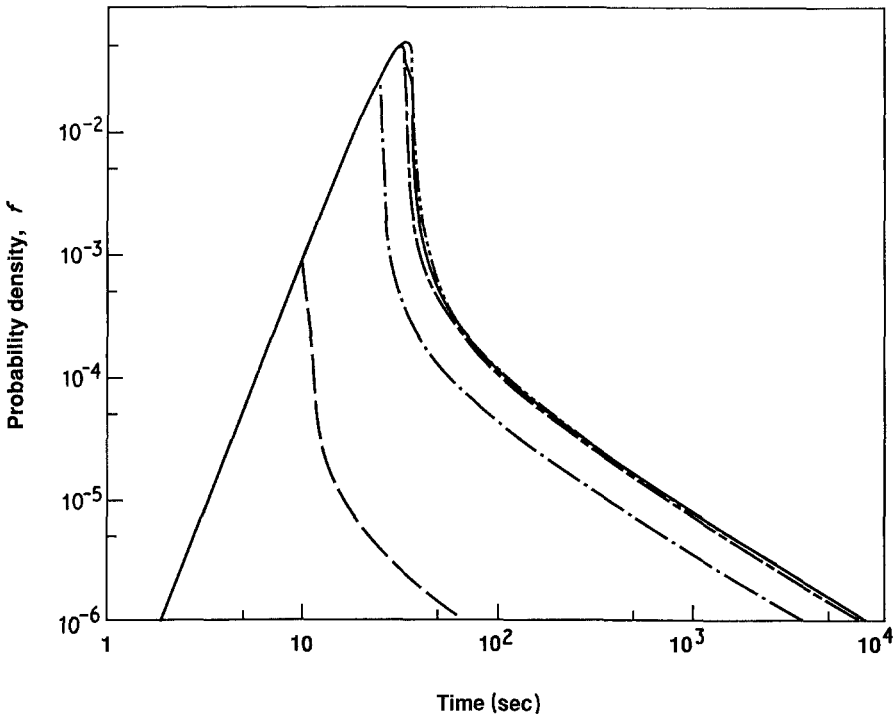

Figure 1 Lifetime density function for stress ratio ϕ = (– – –) 0.30, (–·–) 0.70, (– – –) 0.925, (——) 1.00 and (—·—·—) 1.05. $\varrho = 250, \eta = 5, \sigma_R = 4000$ MPa, $R = 120$ MPa sec^{-1}.

function (Equation 22), for the fibres as high as possible between the loading time t_0 and the censor time t_C, the time of termination of the experiment. Indeed, when the density is large, the increase in probability of failure between t_0 and t_C will be large, and failures are most likely to be observed. The censor time t_C is obviously limited by practical considerations.

In Fig. 1 the density function Equation 22 is plotted against time for the stress ratios $\phi = 0.30, 0.70, 0.925$, 1.00 and 1.05. For this example, a power-law exponent $\varrho = 250$, respective shape and scale parameters of 5 and 4000 MPa for strength, and a loading rate of 120 MPa sec^{-1} are used. These values are comparable to those in the experiments described later.

Over the time range shown, the density increases as the stress level σ increases, but the rate of increase falls off at ϕ near 1.0, that is for stress levels close to the value of the Weibull scale parameter for strength. At the three highest stress levels the density functions appear to be effectively identical soon after loading. However, by maximizing the density function Equation 22 with respect to σ and using Equation 16, an exact expression for the optimal stress ratio ϕ_t for each time point is obtained,

$$\phi_t = [t(\varrho + 1)/t_R]^{-1/\varrho} \quad (24)$$

For larger times the optimal stress actually drops, but very slowly when ϱ is very large. This minor effect is barely evident in the upper tails of the plots on Fig. 1.

2.8. Stepwise lifetime testing

As discussed later, the tabbing procedure for fibre specimens was necessarily tedious and complicated. In order to maximize the amount of information from a single sample of specimens and minimize the possibility of sample-to-sample variations, a stepwise loading procedure was used. By this procedure, a sample of specimens is subject to the stress history of Equation 17 at stress level σ_1, and then unloaded after a suitably long time t_{C1} called the censor time. A second stress level σ_2 is chosen larger than the first, and the surviving specimens are subject again to the stress history (Equation 17) at this new stress level as though they were virgin specimens. Again the specimens are unloaded after a suitably long time t_{C2}. The process is repeated at a third stress level and so on.

The critical factor is to increase sufficiently the stress level at each step to ensure that the effect of the previous stress history is negligible at the new stress level. In essence, this means that the value of the integral in Equation 4 for all past stress histories is insignificant compared with its value upon loading up to the newest stress level σ using the stress history of Equation 17. Note that ϱ must be very large for this phenomenon to occur. Using this stepwise procedure, the sample of fibres can be treated as essentially virgin at each new stress level. Moreover, the cumulative number of failures at the start of the steady-load portion of each stress level can be compared with the predicted number based on the experimentally determined strength distribution.

To determine a suitable stress level at each new step the fraction of initial failures is evaluated using the strength distribution of Equation 12. This number must be greater than the fraction of lifetime failures predicted using the lifetime distribution (Equation 19) at the time t_C of censoring the experiment for the previous stress level. Calculation of this fraction requires an assumed value for the power-law exponent ϱ which must be no larger than the value of ϱ estimated eventually from the experiments.

3. Experiments

3.1. Background

The experimental work consisted of both tension tests on single graphite fibres to determine their strength statistics, and creep-rupture tests on single graphite fibres at three stress levels to determine their lifetime statistics. The data were in turn used to establish estimates for the Weibull shape and scale parameters

for both strength and lifetime as well as the power-law exponent ϱ.

Hercules IM6 graphite fibres were used throughout the tests. These fibres were from the same spool (a 12 000-fibre tow) as used in previous studies of seven-fibre microcomposites at our laboratory [5]. The fibres were nominally 5.5 μm in diameter and a gauge length of 5 cm was used for all tests. Hercules IM6 fibres have a modulus of elasticity of 280 GPa, and the Weibull scale parameter for strength is typically about 4000 MPa. The fibres were unsized in order to facilitate separating individual fibres from the tow. All tests were performed at standard conditions (21° C, 50% r.h.).

In the preliminary experiments the tabbing techniques and tension test procedures used were similar to those of Phoenix *et al.* [5]. Although satisfactory for tension tests, the paper and cyanoacrylate adhesive tabbing technique itself proved to be subject to creep rupture and time-dependent distortion and therefore required modification. The creep-rupture testing equipment developed by Wagner *et al.* [10] for testing Kevlar 49 fibres and later used by Wu *et al.* [11] was used during the preliminary experiments. However, additional isolation from dynamic overloads proved necessary for the graphite fibres because of the expected large inherent value of ϱ (about eight times that for Kevlar 49). For the experimental results presented here refined procedures were used, and it is the refinements that will be emphasized.

3.2. Sample preparation

The fibres were separated from the 12 000-fibre tow by placing a 50 cm section in a distilled water bath and agitating the water. The fibres were touched only at their ends, drawn out of the tow, and place on a Teflon-coated board. A total of 55 fibres 50 cm long were extracted from six different cross-sections of the tow.

A specially designed vibroscope [12] was used to measure the diameter of a 5 cm section of each 50 cm fibre. The coefficient of variation along the length of the fibre was found to be about 4.0% in previous studies [5], so the 5 cm section was considered representative of the entire 50 cm length.

Two metal tabs were glued on paper templates which established the 5 cm gauge length. A 15 cm section of fibre under slight tension was placed across the gauge section on top of the metal tabs. A 5 cm length of cotton thread that extended outside the gauge section was placed on the tab coaxially with the fibre. The tabs were square in cross-section but with a V-shaped groove machined along the length to facilitate alignment. They were designed so that when hanging vertically from the cotton thread their centre of gravity would be coaxial with the fibre. The cotton thread had negligible flexural stiffness and was unable to exert a bending moment on the hanging metal tab. A total of 110 specimens were prepared and assigned numbers in the sequence of preparation.

The fibre and thread were glued to the metal tab using an epoxy blend of 60% Dow DER 732, 40% Dow DER 332, and Dow DEH 26 hardener. The epoxy was heated to about 50° C while mixing to lower the viscosity. The epoxy was cured at 100° C for 4 h and then cooled slowly.

The metal/epoxy tabs were not subject to the failures afflicting the paper/cyanoacrylate tabs during preliminary creep-rupture tests. Examples of failures with paper/cyanoacrylate tabs were a fibre breaking well inside the tab due to debonding or voids in the glue, or a fibre breaking at the entrance to the tab due to curling of the tab with age. These types of failure were not observed with the metal/epoxy tabs.

3.3. Tension tests

A list of 110 random integers was generated in order to select specimens for the tension tests and the creep-rupture tests. 55 specimens were selected for the tension tests which were performed on an Instron Model 1130 constant-rate-of-displacement machine. The crosshead speed was 0.02 mm sec^{-1} which produced a loading rate of about 120 MPa sec^{-1}. Each specimen was clamped by the cotton threads and the paper template was cut away. Load–displacement curves were generated which showed brittle behaviour and no evidence of debonding in the tabs, and the breaking strengths were calculated as the peak loads. Every effort was made to duplicate the clamping situation to be used in the creep-rupture tests to avoid any differences due to clamping effects. Five specimens were accidently destroyed in handling so that 50 successful tension tests were performed.

From the vibroscope experiments, the mean diameter of the fibre specimens was found to be 5.5 μm with a c.v. (coefficient of variation, or standard deviation divided by the mean) of 4.7%. The failure stress for each fibre specimen was calculated using the cross-sectional area of the extracted fibre which was used to make that specimen. The results are plotted on Weibull probability paper (Fig. 2) using the maximum likelihood estimation (MLE) technique [13]. As shown, the MLE-derived Weibull distribution fits well to the 50 data points. The estimates of the Weibull shape and scale parameters η and σ_R, were 4.6 and 4340 MPa, respectively, at a 5 cm gauge length.

The basic statistics and estimates for the tension tests are shown in Table I. As mentioned earlier, considerable development was involved in arriving at a suitable tabbing technique, especially for the creep-rupture tests. For comparison purposes, Table I also shows earlier results using paper tabs with a

TABLE I Strength statistics for Hercules IM6 graphite fibres (5 cm gauge length)

Tabbing technique	Mean area (μm^2) + (c.v.)	Mean stress (MPa) + (c.v.)	Scale parameter (MPa)	Shape parameter
Paper/cyanoacrylate [5]	24.2 (6.6)	3730 (25.7)	4099	4.3
Metal/epoxy	24.9 (6.8)	3955 (25.2)	4340	4.6

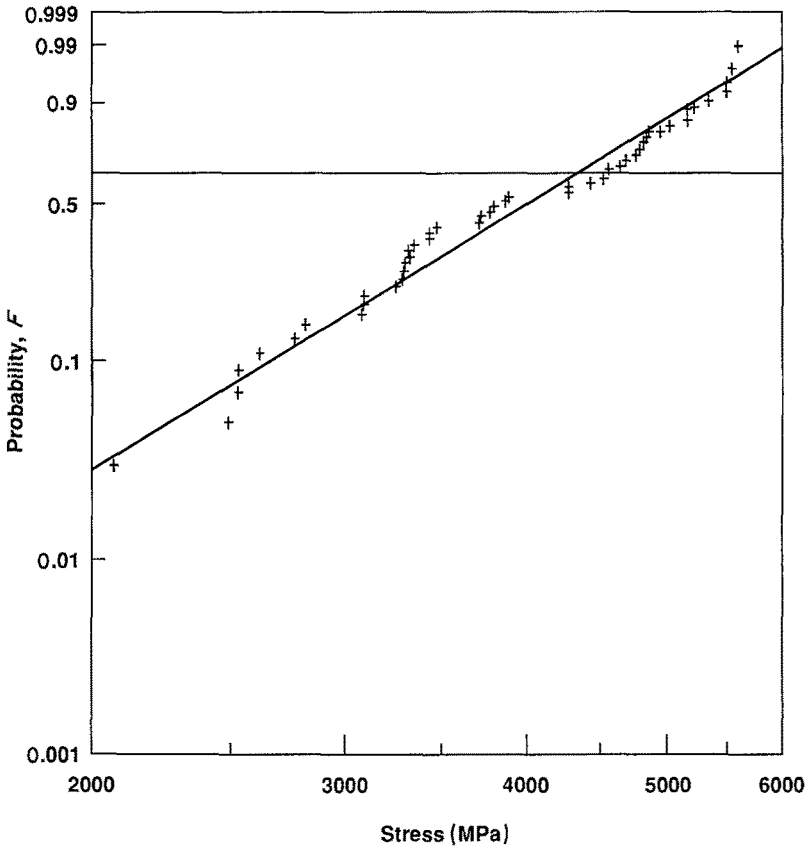

Figure 2 Fibre strength plotted on Weibull probability coordinates. Gauge length = 5 cm, $\eta = 4.6$, $\sigma_R = 4340$ MPa.

cyanoacrylate adhesive. The lower tails of the two distributions for the two techniques were about the same, but at higher failure stresses the paper tab system appeared to produce inferior strengths.

3.4. Creep-rupture tests

As mentioned, the creep-rupture apparatus (Fig. 3) was a modified version of the 25-station rack used by Wagner *et al.* [10] and later by Wu *et al.* [11]. In the original apparatus, the fibres were suspended vertically from top-mounted switches. Weights were placed on a sheet-metal lowering tray and then attached to the bottom tabs of the fibres. The tray was then lowered by a motorized cable system, and the times to failure were recorded with a microcomputer-based system.

Considerable modification to this equipment was required for testing graphite fibres. In particular, greatly improved vibration isolation and slower loading rates were necessary in order to measure the lifetime phenomena of interest. The basic apparatus was structurally stiffened and increased in mass to 250 kg. The lowering tray was replaced with a massive Teflon-covered platform constructed of plywood in a steel frame. The whole apparatus was mounted on a vibration isolation table consisting of a 650 kg granite slab and four low-pressure pneumatic springs. The resonant frequency of the system was approximately 2 Hz, so that thread lengths for the tabs were selected to avoid resonance at this frequency. The apparatus was shielded from convective air currents in the room. The motor only operated while lowering the table and

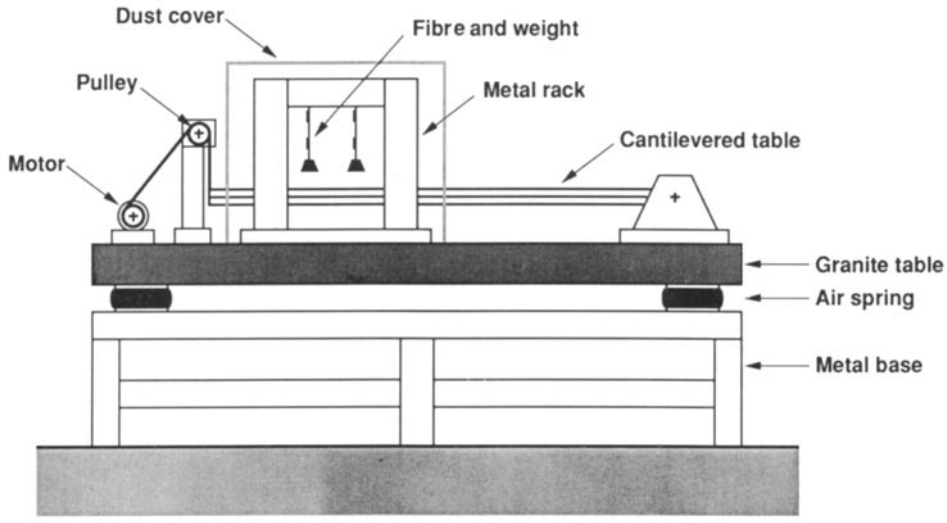

Figure 3 Schematic diagram of creep-rupture apparatus.

the system seemed to be most free of vibration with the motor mounted on the granite slab.

Preliminary experiments showed that contact bounce in the switches due to specimen failure could cause sufficient vibration to disturb neighbouring specimens. In consideration of the fact that fibre failures are widely spaced after the first few minutes of the test, the failure times were recorded manually through frequent visual checks of the experiment. This approach provided satisfactory resolution of the failure times.

From the preliminary study mentioned in Section 2.7, three stress ratios $\phi = \sigma/\sigma_R$ were chosen for the creep-rupture tests. These stress ratios were 0.925, 1.00 and 1.05, and were based on $\sigma_R = 4340\,\text{MPa}$.

For the first stress ratio of 0.925 all 55 remaining fibre specimens were to be tested for creep rupture using specially tailored weights as in Wu *et al.* [11]. In order to maximize the number of specimens hanging in the 25-station apparatus shortly after loading (avoiding the necessity of having more than one run of the experiment) all specimens were prestressed to $0.925\sigma_R$ in the Instron tension test machine. From the strength distribution it was calculated that about 50% of the specimens would fail due to this pre-testing. This procedure was rather tedious and delicate, and seven specimens were accidentally destroyed during handling. Of the 48 remaining, 23 failed in this pre-testing, which is just short of the 50% expected. The remaining 25 survivors were placed in the creep-rupture apparatus.

Upon loading to the stress ratio 0.925 (loading rate of 120 MPa sec^{-1}) one of the 25 specimens failed at the start (that is, its failure time was too short to resolve) and four failed in the creep rupture. The test was censored after 168 hours (one week), and the 20 surviving specimens were unloaded by raising the platform.

Next, weights were prepared for loading the 20 survivors at the stress ratio 1.00 and carefully attached to the bottom tabs with the top tabs remaining in position. Again the process was tedious and two specimens were destroyed by handling, leaving 18 for the creep-rupture test. One specimen failed on loading (or at a time too short to resolve) and four specimens failed in creep rupture. The experiment was censored after 72 h and the 13 surviving specimens unloaded by raising the platform.

Lastly, weights for loading at the stress ratio 1.05 were prepared for the 13 survivors and attached as before. Two specimens were again destroyed by handling, leaving 11 for the creep-rupture test. Three failures occurred on loading, or at times too short to resolve, and two others failed in creep rupture up to the censor time of 336 h. Thus a total of six specimens survived all testing.

4. Analysis for individual data sets

4.1. Adjusted sample size for creep-rupture tests

As explained in Section 2.8, by raising the load sufficiently at each step, the creep-rupture test at each stress level could be considered to be essentially equivalent to a test on a virgin sample of 48 specimens, though the full likelihood analysis presented later relaxes this assumption. For each stress level, the number of failures on loading could be calculated as the cumulative number of the original 48 that had failed up to that point, and the lifetime of creep-rupture failures could be measured from that point. Determining the fraction of failures on loading for each stage, however, was complicated by the fact that four handling failures had occurred as discussed previously. The appropriate procedure was to calculate an adjusted sample size for each stress level by multiplying the adjusted sample size for the previous stress level by the fraction of the creep-rupture survivors that were not destroyed in handling, and to take the closest integer. At the end of the creep-rupture test at the first stress level, 20 survived but two of these were destroyed during handling leaving 18, or the fraction 9/10.

By this procedure, the adjusted sample size for the first stress ratio of 0.925 is 48. The adjusted sample size for the second stress ratio 1.00 is the closest integer to $48 \times (18/20)$ or 43. For the third stress ratio 1.05, there were 13 creep-rupture survivors of the second stress level of which two were destroyed by handling, leaving 11. The adjusted sample size is the closest integer to $43 \times (11/13)$ or 36.

4.2. Actual and predicted failures on loading

It is useful to compare the failures on loading calculated from the creep-rupture experiments with those predicted from the tension test results discussed earlier. In this calculation it is necessary to take the handling failures into account by working with the adjusted sample sizes. At a stress ratio of 0.925 the predicted fraction of failures from the tension tests, using Equation 12, is 0.50 and from the above discussion $(23 + 1)/48 = 0.50$ is calculated which agrees. At the stress ratio 1.00 the adjusted sample size in the creep-rupture test was 43 with 17 surviving in creep rupture to measurable times, so that the adjusted fraction of initial failures is $(43 - 17)/43 = 0.60$. This compares favourably with 0.63 from the tension tests as calculated using Equation 12.

Lastly, at the stress ratio 1.05 the predicted fraction of initial failures from the tension tests is 0.71. The adjusted sample size is 36 and there were 11 specimens actually loaded in the creep-rupture apparatus with three of these failing at times too short to measure. The adjusted fraction of failures just after loading is $[36 - (11 - 3)]/36 = 0.77$, whereas the predicted fraction is 0.71. Observers of the experiment noted that only two of the three failures were obvious loading failures; the other one occurred at or possibly just after full loading. The possibility of a smaller fraction of initial failures (in closer agreement with the tension test results) is considered in a later analysis. The actual fraction (based on the adjusted sample size) and the predicted fraction (based on the tension test) of failures on loading for the three stress levels are shown in Table II. Also shown is the actual fraction at the stress ratio 1.05 based on one less initial failure.

In view of the uncertainty just mentioned, and the predicted behaviour of the failure rate (density) in

TABLE II Adjusted sample sizes and actual and predicted fraction of failures on loading

Stress ratio, $\phi = \sigma/\sigma_R$	Adjusted sample size	Actual fraction	Predicted fraction
0.925	48	0.50	0.50
1.00	43	0.60	0.63
1.05	36	0.77*	0.71

*0.75 if based on one less loading failure and 0.72 if based on two less loading failures.

Fig. 1, which for the stress ratio 1.05 is most elevated at the shorter times just after loading, the experimental results are quite reasonable. The deviations from the predictions are probably due to chance alone. Nevertheless, later estimates from the results at the highest stress level do have increased uncertainty because of the smaller adjusted sample size and the smaller number of survivors on test.

4.3. Analysis of lifetime data

The creep-rupture experiments began with a ramp loading for about 35 sec, requiring Equation 18 or 19 as a model. Further study shows that if time is measured from $t_R^* = t_0\varrho/(\varrho + 1)$ then Equations 18 and 19 are exactly Weibull distributions for all $t \geqslant t_0$. The time t_R^* differs from t_0, the time of full loading, by the amount $t_0/(\varrho + 1)$ which is almost negligible since ϱ is anticipated to be very large (> 200). In this case $t_0/(\varrho + 1)$ is about 0.2 sec (far less than our actual resolution time discussed shortly). Note that $t_0/(\varrho + 1)$ is interpreted to be the time under constant stress σ which would cause the same probability of failure as the ramp loading up to $t_0 = \phi t_R$.

As mentioned, the failure times were measured manually so that it was possible to resolve early failures only to within about two seconds. This error in itself is considerably larger than the time shift $t_0/(\varrho + 1)$ above. Also the specimens had all seen a past stress history before being loaded in the creep-rupture experiment. Nevertheless, because of the large anticipated value of ϱ it is quickly seen from Equation 4 that time spent at all previous stress levels is equivalent to a fraction of a second at the newest stress level (except for the highest stress level as noted shortly).

Thus, in this first MLE analysis, the data were analysed one stress level at a time using the Weibull distribution (Equation 9) where lifetime is measured conceptually from the instant t_R^*. The failures on loading were actually assigned to an interval $(0, t_0^*)$ where t_0^* is a constant to be specified, but lifetime failures were assigned their exact failure times. (These failure times, which were all at least a few minutes, were actually measured from the time point t_0, but the difference is insignificant as it is much less than the resolution time.) The survivors at the time of censoring t_C were assigned to the interval (t_C, ∞). In principle t_0^* would be taken as $t_0/(\varrho + 1)$, but in reality some "initial" failures were really failures which had lifetimes too short to detect, so $t_0^* = 2.0$ sec was chosen more in line with the resolution time of the experiment. The MLE procedure that was used could accommodate interval and censored data of this type [13]. In all cases adjusted sample sizes were used, as shown in Table II. The Weibull parameters for the three stress levels are shown in Table III together with power-law exponent values ϱ as calculated from Equation 13.

TABLE III Lifetime parameter estimates at each stress level with the resolution time $t_0^* = 2.0$ sec

Stress ratio, $\phi = \sigma/\sigma_R$	Fraction of loading failures	Shape parameter, $\hat{\beta}$	Scale parameter, $\hat{t}_\sigma$ (sec)	Power-law exponent†, $\hat{\varrho}$
1.05	28/36	0.013	5.14×10^{-14}	354
	27/36*	0.019	9.21×10^{-8}	236
1.00	26/43	0.022	7.30×10^{1}	212
0.925	24/48	0.019	8.00×10^{8}	245

*Based on assigning one failure to the interval (2 sec, 4 sec).
†Based on Equation 13.

The predicted value of ϱ seemed inordinately large at the 1.05 stress ratio and β seemed small. The data were reanalysed from the viewpoint that one of the initial failures at this stress ratio may have occurred a second or two after the ramp loading was completed. It was also determined, using Equation 4, that the effect of loading over time at the previous stress ratio 1.00 actually was equivalent to about 2 sec of time at the stress ratio 1.05 (assuming $\varrho = 250$). The MLE analysis was repeated and one of the 28 "initial" failures was assigned to a time interval (2 sec, 4 sec) with the remaining 27 assigned to the interval (0 sec, 2 sec). The results of this second analysis are also shown in Table III. With this approach, the values of both the Weibull shape and scale parameters are more consistent, in the context of the model, with the results from the two lower stress levels and the tension test.

Fig. 4 shows the lifetime data at the three stress levels together with the MLE-fitted Weibull distributions. Also shown are the fractions of initial failures and the fractions surviving at the time of censoring. The adjusted sample sizes were used for all plotting and only the second of the two analyses at the 1.05 stress ratio is shown.

To assess the effect of the choice of the resolution time constant t_0^* on the results, the analysis was repeated for t_0^* values of 0.5 and 5.0 sec. The corresponding intervals for the 28th failure at the 1.05 stress ratio are (0.5 sec, 2.5 sec) and (5.0 sec, 7.0 sec). The results are shown in Table IV where again Equation 13 was used to calculate ϱ. Increasing t_0^* has the effect of diminishing the estimated value of ϱ.

The effect of stress level on the Weibull scale

TABLE IV Lifetime parameter estimates with the resolution time $t_0^* = 0.5$ and 5.0 sec

Resolution time, t_0^* (sec)	Stress ratio, $\phi = \sigma/\sigma_R$	Shape parameter, $\hat{\beta}$	Scale parameter, $\hat{t}_\sigma$ (sec)	Power-law exponent†, $\hat{\varrho}$
0.5	1.05*	0.018	3.76×10^{-9}	262
	1.00	0.019	3.06×10^{1}	237
	0.925	0.017	1.78×10^{9}	271
5.0	1.05*	0.021	7.52×10^{-7}	219
	1.00	0.023	1.30×10^{2}	200
	0.925	0.020	4.39×10^{8}	227

*Based on assigning one failure to the interval (t_0^* sec, $t_0^* + 2$ sec).
†Based on Equation 13.

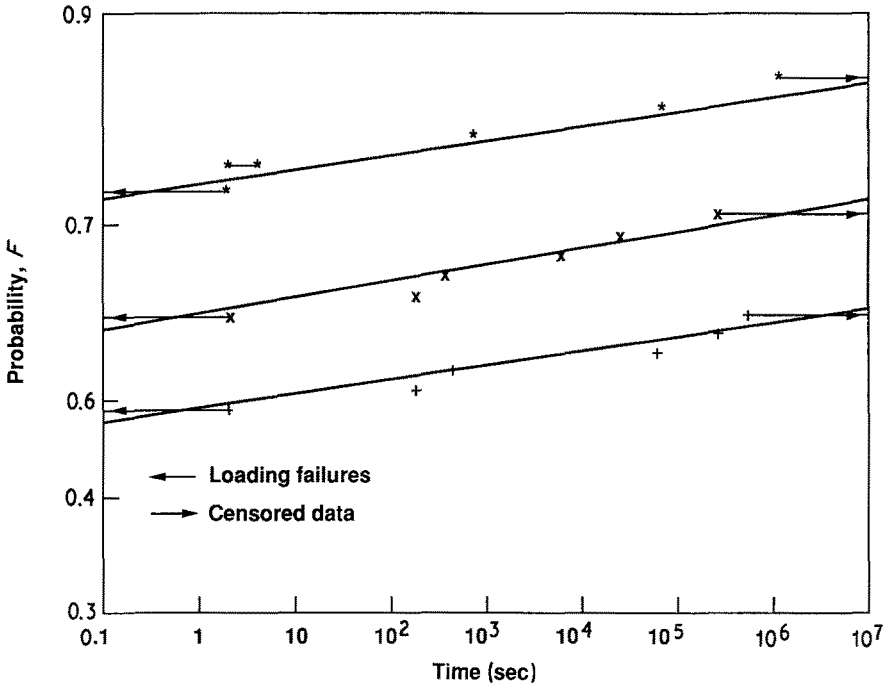

Figure 4 Fibre lifetimes at stress ratio ϕ = (+) 0.925, (×) 1.00 and (★) 1.05 on Weibull probability coordinates.

parameter for lifetime is shown in Fig. 5 which uses log–log coordinates. On this scaling, the slope of the line fitted to the parameter values is $-1/\varrho$. The estimates for ϱ are 326, 294 and 272 for resolution times t_0^* of 0.5, 2.0 and 5.0 sec intervals, respectively. The straight line is a least-squares fit corresponding to the t_0^* = 2.0 sec data (with the above-mentioned interval adjustment at ϕ = 1.05).

Note in Fig. 5 that the horizontal position of the value for the Weibull scale parameter for lifetime, t_σ, at a given stress level is strongly influenced by the fraction of initial failures at that stress level. This is apparent from Fig. 4, where one can appreciate that an unusually high number of initial failures will tend to raise the fitted line, thereby reducing the estimate of t_σ, and vice versa. As compared with the predicted fractions from the strength tests, the actual fractions listed in Table II are consistent with t_σ being to the right of the line in Fig. 5 at σ = 4340 MPa (ϕ = 1.00) and being to the left at σ = 4557 MPa (ϕ = 1.05), thus causing curvature. An improved estimating procedure which takes into account both the strength results and the lifetime results at the same time is presented in the next section.

5. Full likelihood analysis

5.1. Likelihood function

The analysis in Section 4 is based on well-established maximum likelihood techniques for fitting the Weibull distribution, applied separately to each of the stages of

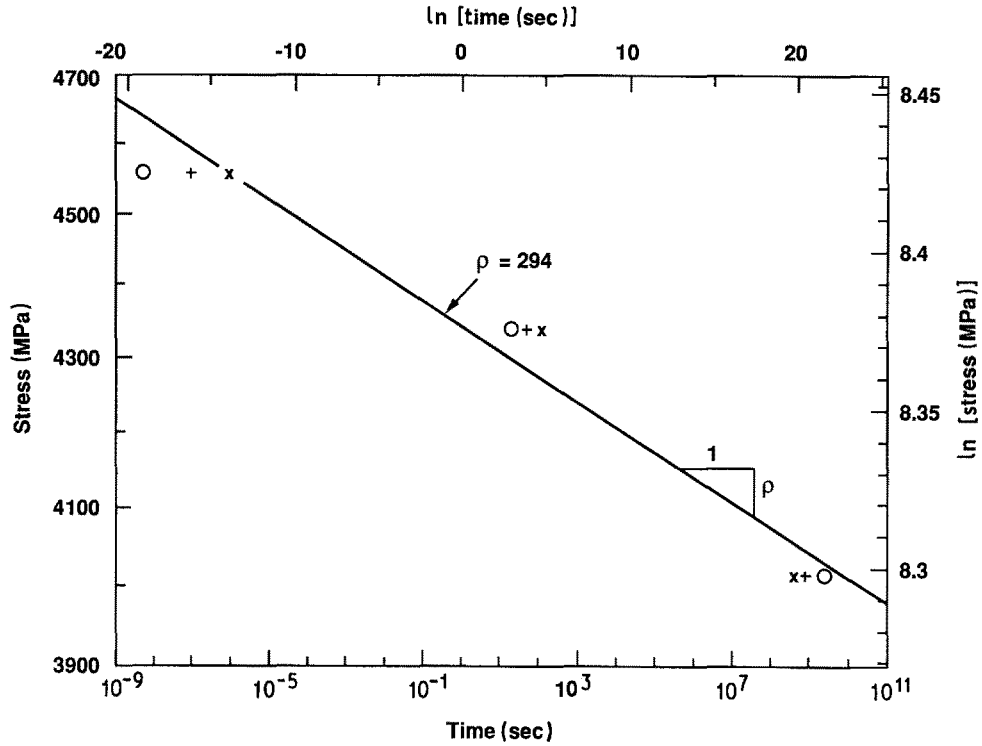

Figure 5 Weibull scale parameter for lifetime against stress level on power-law coordinates for t_0^* = (O) 0.5 sec, (+) 2.0 sec (ϱ = 294) and (×) 5.0 sec.

the experiment. One advantage of analysing the data this way is that by comparing the results obtained from the different stages of the experiment, a check is provided on the suitability of the model being fitted. Nevertheless, if the validity of the model (Equation 4) is assumed, then it is possible to obtain more precise estimates of the parameters (including confidence intervals) by a full likelihood analysis, in which the whole set of data is treated as a single entity and a likelihood function is constructed to represent the whole experiment.

First, Equation 4 is written using η and σ_R defined by Equations 13 and 14 as follows,

$$F(t; \boldsymbol{\sigma}) = 1 - \exp\left\{-\left[R(\varrho + 1)\int_0^t \sigma(u)^\varrho \, du\right]^{\eta/(\varrho+1)} \sigma_R^{-\eta}\right\} \quad (25)$$

For a fibre which is known to have failed at time t_F, the contribution to the likelihood function is

$$f(t_F; \boldsymbol{\sigma}) = \mathrm{d}[F(t_F; \boldsymbol{\sigma})]/\mathrm{d}t_F \quad (26)$$

In our experiments, the exact time to failure for some fibres is unknown and only the fact that the failure occurred between times t_{F1} and t_{F2} is recorded. This includes fibres which were still surviving at the end of the experiment, and those which were accidentally lost during the course of the experiment. In these cases $t_{F2} = +\infty$. The contribution to the likelihood is

$$F(t_{F2}; \boldsymbol{\sigma}) - F(t_{F1}; \boldsymbol{\sigma}) \quad (27)$$

The full likelihood is constructed by multiplying together Equations 26 and 27 for each of the 98 fibres for which data are available (i.e. including both the initial tension tests and the lifetime tests, but excluding the five tension test fibres and the seven lifetime test fibres which were broken before any testing could be performed). This likelihood function depends on the three parameters σ_R, η and ϱ, and is therefore denoted

$$\text{Likelihood function} = L(\sigma_R, \eta, \varrho) \quad (28)$$

In order to evaluate Equation 25, the parts of the experiment during which the fibres were unloaded were ignored, since no fibre failures (other than accidental breaks) occurred during such periods. This simplified the analysis, and the assumed stress history $\sigma(u)$ was

$$\sigma(u) = \begin{cases} Ru & 0 < u < \sigma_1/R \\ \sigma_1 & (\sigma_1/R) < u < t_1 \\ \sigma_1 + R(u - t_{C1}) & t_1 < u < [t_1 + (\sigma_2 - \sigma_1)/R] \\ \sigma_2 & [t_1 + (\sigma_2 - \sigma_1)/R] < u < t_2 \\ \sigma_2 + R(u - t_{C2}) & t_2 < u < [t_2 + (\sigma_3 - \sigma_2)/R] \\ \sigma_3 & [t_2 + (\sigma_3 - \sigma_2)/R] < u < \infty \end{cases} \quad (29)$$

with corresponding values for the integral in Equation 25, respectively on each of the above time intervals, given by

$$\int_0^t \sigma(u)^\varrho \, du = \begin{cases} (R^\varrho t^{\varrho+1})/(\varrho + 1) \\ \sigma_1^{\varrho+1}/[R(\varrho + 1)] + \sigma_1^\varrho[t - (\sigma_1/R)] \\ \sigma_1^\varrho[t_1 - (\sigma_1/R)] \\ \quad + [\sigma_1 + R(t - t_1)]^{\varrho+1}/[R(\varrho + 1)] \\ \sigma_1^\varrho[t_1 - (\sigma_1/R)] \\ \quad + \sigma_2^\varrho\{t - t_1 - (\sigma_2/R)[\varrho/(\varrho + 1)] \\ \quad + (\sigma_1/R)\} \\ \sigma_1^\varrho[t_1 - (\sigma_1/R)] \\ \quad + \sigma_2^\varrho\{t_2 - t_1 - [(\sigma_2 - \sigma_1)/R]\} \\ \quad + \{\sigma_2 + R(t - t_2)\}^{\varrho+1}/[R(\varrho + 1)] \\ \sigma_1^\varrho[t_1 - (\sigma_1/R)] \\ \quad + \sigma_2^\varrho[t_2 - t_1 - (\sigma_2 - \sigma_1)/R] \\ \quad + \sigma_3^\varrho\{t - t_2 - (\sigma_3/R)[\varrho/(\varrho + 1)] \\ \quad + (\sigma_2/R)\} \end{cases} \quad (30)$$

where $t_1 = t_{C1} + (\sigma_1/R)$ and $t_2 = t_1 + [(\sigma_2 - \sigma_1)/R] + t_{C2}$ and with t_{C1} and t_{C2} the censor times defined earlier. These values may be substituted into Equation 25 to give an explicit formula for the required distribution function.

In the case of fibres which fail during the initial loading stage (i.e. $t < \sigma_1/R$), the distribution of failure time is given by

$$F(t; \boldsymbol{\sigma}) = 1 - \exp\left[-(Rt/\sigma_R)^\eta\right] \quad (31)$$

or, equivalently, the distribution of failure stress $\sigma = Rt$ is given by

$$F^*(\sigma; \sigma_R, \eta) = 1 - \exp\left[-(\sigma/\sigma_R)^\eta\right] \quad (32)$$

with density

$$f^*(\sigma; \sigma_R, \eta) = (\eta/\sigma_R)(\sigma/\sigma_R)^{\eta-1} \exp\left[-(\sigma/\sigma_R)^\eta\right] \quad (33)$$

consistent with Equation 12. For these fibres it makes no difference whether Equations 26 and 31 are used or Equation 33 is used, but to be consistent with the method used earlier for the analysis of tension test data, Equation 33 is used. Thus Equation 33 applies for the fibres of the initial tension tests. For all these fibres the exact failure stresses were known so that intervals were not needed.

In the case of the fibres which failed during the life-testing stage of the experiment, lower and upper bounds were set for the individual failure times t_{F1} and t_{F2}, so as to apply Equation 27. Coding the data in this way enabled testing the sensitivity of the results to certain data items, particularly for those fibres which failed on loading at each stage, by varying t_{F2} to represent the different guesses of the upper bound on failure time (corresponding essentially to t_0^* in Section 4.3). For failures during the constant-load parts of the experiments the intervals were set to be very narrow

($\pm 0.1\%$ of the actual failure times). A sensitivity study showed that varying the width about that order had absolutely no effect on the results.

5.2. Numerical procedures

The likelihood function was maximized using a variant on the standard Newton–Raphson algorithm. More precisely, the log likelihood function was written as a function of three parameters $\log \sigma_R$, $\log \eta$ and $\log \varrho$, the logarithmic transformation on the parameters being made because, knowing the magnitudes of the numbers involved, this seemed appropriate to guarantee numerical stability. The precise algorithm used was developed specifically for maximum likelihood problems, though in no case was there any serious difficulty in finding the maximum, so a packaged Newton or quasi-Newton routine is expected to work just as well.

As well as giving parameter estimates, it is desirable to obtain confidence intervals. The following two methods were used for this, both of them standard procedures in statistical analysis of this nature.

(i) *Wald's method.* In this method an approximate 95% confidence interval for a parameter is given by

$$\text{parameter estimate} \pm 1.96 \times (\text{standard error of estimate}) \quad (34)$$

where the factor 1.96 is obtained from tables of the normal distribution and the standard error of the ith parameter is the square root of the ith diagonal element of the inverse of the observed information matrix. The observed information matrix is the matrix of second-order derivatives of minus the log likelihood function, evaluated at the maximum likelihood estimates. In our case a logarithmic transformation was applied to the original parameters, so the confidence intervals are calculated on a logarithmic scale, and then transformed back to produce confidence intervals for the original parameters.

(ii) *Likelihood ratio method.* This method is more computationally intensive than Wald's method, but gives better results when (as here) the likelihood function is highly skewed. To illustrate its application, suppose ϱ in Equation 28 is the parameter of interest. For each ϱ, define a profile likelihood by maximizing with respect to σ_R and η and conditionally on ϱ, i.e.

$$L^*(\varrho) = \max_{\sigma_R, \eta} L(\sigma_R, \eta, \varrho) \quad (35)$$

Suppose L^* is maximized at $\varrho = \hat{\varrho}$, the maximum likelihood estimate of ϱ. An approximate 95% confidence interval is the set of ϱ for which

$$2 \log [L^*(\hat{\varrho})/L^*(\varrho)] < 3.84 \quad (36)$$

where 3.84 is the upper 5% point of the χ^2 distribution, which is the relevant asymptotic distribution for the quantity on the left-hand side of Equation 36.

The need for an additional maximization in Equation 35 makes the second method more computationally intensive than Wald's method, which requires only one maximization in total, but in the present case the two methods give virtually identical results if Equation 35 is replaced by

$$L^{**} = L(\hat{\sigma}_R, \hat{\eta}, \varrho), \quad (37)$$

in which $\hat{\sigma}_R$ and $\hat{\eta}$ are the overall maximum likelihood estimates of σ_R and η. In other words, to define L^{**} the maximization in Equation 35 is performed only once (at $\varrho = \hat{\varrho}$) instead of separately each time Equation 35 is evaluated.

5.3. Results

For the initial tensile strength data maximum likelihood estimates of $\hat{\sigma}_R = 4339$ and $\hat{\eta} = 4.61$ were found, agreeing with the earlier analysis, and the corresponding confidence intervals were (4080, 4620) and (3.8, 6.0) computed by Wald's method on a logarithmic scale, as described in Section 5.2.

For the analysis of the full data (including the initial tension tests) we considered four cases corresponding to different values of the resolution time t_0^*. For Case I we took $t_0^* = 0$ sec, meaning that failures with unknown times associated with the ramp portion of the loading in Equation 29 were assigned exactly to the time intervals of their respective ramp portions. For Case II we took $t_0^* = 0.5$ sec (except for one specimen on the last ramp loading where we took $t_0^* = 4$ sec for reasons mentioned earlier) to reflect the fact that specimens that failed during the ramp loading could actually have hung under steady load for up to one-half second before failing. Case III was similar to the Case II except that t_0^* was taken as 2 sec (except again for one at 4 sec). For Case IV we took $t_0^* = 5$ sec. In this way we could determine the sensitivity of the estimates to this resolution time t_0^*. Table V lists the estimates of the respective Weibull shape and scale parameters for strength and the power-law exponent ϱ. Table V also lists an estimate for β, the lifetime shape parameter as calculated from $\hat{\eta}$ and $\hat{\varrho}$ using Equation 13. (The Weibull shape parameter for lifetime t_σ may be calculated using Equations 15 and 16.) The most realistic values we

TABLE V Parameter estimates for the model under a full likelihood analysis assuming various values for t_0^*

Case	Resolution time, t_0^* (sec)	Strength shape parameter, $\hat{\eta}$	Strength scale parameter, $\hat{\sigma}_R$ (MPa)	Life shape parameter†, $\hat{\beta}$	Power-law exponent, $\hat{\varrho}$
I	0	4.69	4312	0.0109	428
II	0.5*	4.67	4319	0.0128	365
III	2.0*	4.66	4322	0.0137	340
IV	5.0	4.66	4326	0.0145	321

*One specimen assigned $t_0^* = 4$ sec during last ramp load.
† Based on Equation 13.

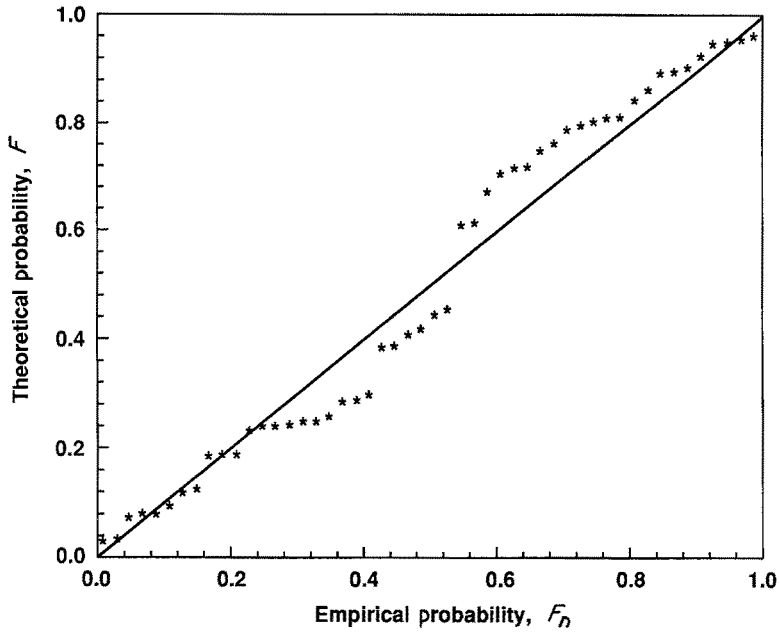

Figure 6 Plot of fitted theoretical Weibull distribution for strength against the Kaplan–Meier empirical distribution function.

believe are those of Case III with $t_0^* = 2$ sec. Clearly the estimate of ϱ (and thus β also) is significantly affected by the choice of t_0^*.

Using the previously described methods we also calculated 95% confidence intervals for the three parameters. For Case III, with our best estimate of $t_0^* = 2.0$ sec, the confidence intervals for the respective parameters $\hat{\sigma}_R$, $\hat{\eta}$, $\hat{\varrho}$ were computed to be (4120, 4535), (3.8, 5.8) and (232, 501) using Wald's method. The confidence intervals for $\hat{\sigma}_R$ and $\hat{\eta}$ are slightly narrower than those from just the strength results, as expected in view of the greater quantity of data being analysed. On the other hand, the confidence interval for $\hat{\varrho}$ obtained from Equation 36 is (250, 555). The difference between this and the confidence interval just quoted for Wald's method is explained by the highly skewed shape of the profile likelihood $L^*(\varrho)/L^*(\hat{\varrho})$, which is an indication that the likelihood ratio method is superior to Wald's method. For the other cases the confidence intervals were virtually the same for $\hat{\eta}$ and $\hat{\sigma}_R$ but for $\hat{\varrho}$ were (316, 694), (268, 595), and (235, 520) respectively for Cases I, II and IV using the likelihood ratio method. Despite the sensitivity of $\hat{\varrho}$ to the resolution time t_0^* there is considerable overlap of the above confidence intervals for $\hat{\varrho}$. Nevertheless the analysis does suggest that the correct value for t_0^* deserves attention in any future experiments.

5.4. Goodness of fit of the model

An obvious question raised by the analysis, especially by the apparent discrepancies in ϱ over different stress levels (Tables II and III, Fig. 5), is how well the model fits the data, i.e. whether the functional form of Equation 25 is adequate to describe the data. We have investigated this by probability plotting, a technique that will now be described.

Let us first ignore the fact that there are some censored observations owing to fibres being broken in handling at various stages of the experiment. Equation 25 tells us, for any fixed t, what is the probability (under the assumed model) that a fibre fails before time t. However, for the particular loading pattern $\sigma(u)$ used in the experiment, we can estimate the function $F(t; \sigma)$ by the empirical distribution function, given by

$$F_n = i/n \qquad Y_i \leqslant t \leqslant Y_{i+1} \tag{38}$$

where $Y_1 < Y_2 < \cdots < Y_n$ are the n ordered failure times of the experiment. A plot of the theoretical distribution $F(t; \sigma)$ against the empirical distribution function $F_n(t)$ therefore provides an indication of the fit of the model. In practice, since the jumps of F_n occur at $t = Y_1, Y_2, \ldots, Y_n$, the plot is evaluated only at those points.

In the case of censored data it is necessary to modify the empirical distribution function to take account of the censoring. The appropriate modification is the Kaplan–Meier (also called Product Limit) estimator, given by

$$F_n(t) = 1 - \prod_{j:t_j<t} (1 - d_j/n_j) \tag{39}$$

where t_j is the jth observed failure time, n_j is the number of current (uncensored) survivors at time t_j, and d_j is the number of observed failures at time t_j. (See Lawless [14].)

For our experimental data, then, the fitted theoretical distribution function was plotted against the empirical distribution function defined by the Kaplan–Meier estimator. This was done separately for the two experiments, i.e. the tensile testing experiment (using Equation 32) where all the fibres were stressed to failure, and the lifetime experiment (using Equation 25 with Equations 29 and 30 and including those fibres which failed during the initial loading). The model parameter values $\hat{\varrho} = 340$, $\hat{\eta} = 4.66$ and $\hat{\sigma}_R = 4322$ MPa were used in each case, and in cases where the failure time was not known exactly but only up to some interval, the midpoint of the interval was used.

Figs 6 and 7 show the resulting plots for the tensile experiment and the lifetime experiment, respectively. If the model is a perfect fit, then the points of the plot should lie very close to the straight line drawn. In Fig.

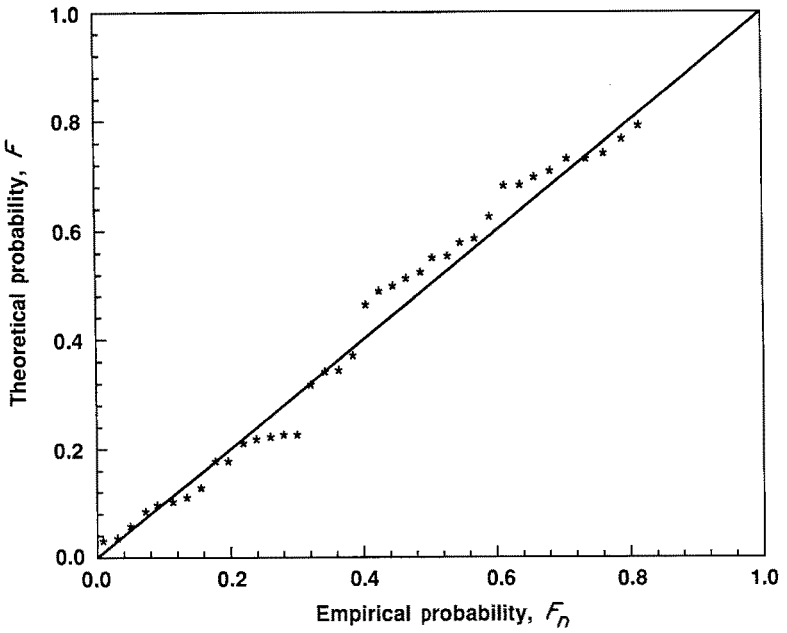

Figure 7 Plot of fitted theoretical lifetime distribution with load steps against the Kaplan–Meier empirical distribution function.

6 there is some discrepancy (plotting points below the theoretical line in the second quarter of the data, and above in the third quarter) but the deviation is well within the confidence limits of the Kolmogorov–Smirnov test. In Fig. 7, the plot stops at the point (0.822, 0.785) which corresponds to the end of the experiment (a few fibres remain unbroken), but the maximum deviation is again insignificant and in fact smaller than in Fig. 6, which corresponds to the Weibull fit to the tensile strength data.

The conclusion is that there is no evidence in the data to contradict the fitted model and that the uncertainty in a few of the observations, although affecting the estimate of ϱ, does not in fact make much difference to the fitted model.

6. Conclusions

With proper care in experimental technique and the use of the appropriate statistical model and analysis procedures, it is possible to measure the creep-rupture performance of graphite fibres. Pre-testing of the fibres and the stepwise procedure for application of the load proved successful in providing significant information from a relatively small number of fibre specimens – about one-third the number that would have been required by conventional procedures. This saving is significant in view of the cost and tedium of preparing samples and the risk of introducing extraneous effects when preparing and testing specimens in groups.

From an overall view of the results it appears that, at ambient conditions (21° C, 50% r.h.), the lifetime of single Hercules IM6 graphite fibres follows a Weibull distribution with a shape parameter value of about 0.016, a value which is about one-tenth that observed for Kevlar 49 fibres [10, 11]. This corresponds to a huge coefficient of variation of about 5000%. The power-law exponent ϱ relating lifetime to load level (Equation 10) is about 300 but may be as low as 250. In future experiments it would be desirable to improve the time resolution of the shortest times, and in the step-up approach to space the stress levels further apart to reduce memory effects at the shortest times. It would also be desirable to increase the sample size, and to run separate experiments at each stress level.

Finally, in the molecular model described in Section 2.1, Equation 7 and the approximation $\tilde{U}_0 = 0.40U_0$ are used to calculate an activation energy U_0 of about 440 kcal mol^{-1} (1840 kJ mol^{-1}) corresponding to $\varrho = 300$. This value is about five times the energy usually associated with scission of a single C–C bond, which is the critical bonding in graphite. Even $\varrho = 200$ yields $U_0 = 296$ kcal mol^{-1} (1240 kJ mol^{-1}). A possible reason is that, because of the strong lateral coupling between atoms in graphite fibres (C–C bonds instead of the weaker hydrogen bonds and Van der Waals forces typical of bonding in polymeric fibres), cooperative coupling between bonds during failure actually occurs, so that several simultaneous C–C bond failures are needed in the crack initiation process. This would also lead to an apparent increase in the activation energy U_0 in the model of Phoenix and Tierney [7].

Acknowledgement

The experimental work was supported by the Cornell Materials Science Center, an NSF DMR-MRL. The mathematical models and statistical techniques were developed under support from the Mathematical Sciences Institute of Cornell University, sponsored by the U.S. Army Research Office.

References

1. R. L. MOORE, M. A. HAMSTAD and T. T. CHIAO, *Fukugo Zairyo: Compos. Mater. Struct.* **3** (1974) 19.
2. Y. KAWAZU, T. NORITA and M. FUJIWARA, *Sen-i Gakkai-shi* **31** (1975) 67.
3. E. M. WU, private communication on unpublished data from Lawrence Livermore National Laboratory (1986).
4. J. T. SHAFFER, in "Materials for Space–The Gathering Momentum", SAMPE Technical Conference, Seattle, 1986, edited by J. T. Hoggatt, S. G. Hill and J. C. Johnson.
5. S. L. PHOENIX, P. SCHWARTZ and H. H. ROBINSON, *Comp. Sci. Tech.* **32** (1988) 81.
6. B. D. COLEMAN, *J. Appl. Phys.* **29** (1958) 968.

7. S. L. PHOENIX and L. J. TIERNEY, *Eng. Fract. Mech.* **18** (1983) 193.
8. S. L. PHOENIX, in Proceedings of 9th US National Congress of Applied Mechanics, Cornell University, Ithaca, New York, 21–25 June, 1982, Book No. H00228 (American Society of Mechanical Engineers, New York, 1982) p. 219.
9. S. L. PHOENIX and C. C. KUO, in "1983 Advances in Aerospace Structures, Materials and Dynamics AD-06", Book No. H00272 (American Society of Mechanical Engineers, New York, 1983) p. 169.
10. H. D. WAGNER, P. SCHWARTZ and S. L. PHOENIX, *J. Mater. Sci.* **21** (1986) 1868.
11. H. F. WU, S. L. PHOENIX and P. SCHWARTZ, *ibid.* **23** (1988) 1851.
12. H. H. ROBINSON, H. F. WU, M. AMES and P. SCHWARTZ, *Rev. Sci. Instrum.* **58** (1987) 436.
13. A. C. COHEN, *Technometrics* **7** (1965) 579.
14. J. LAWLESS, in "Statistical Models and Methods for Lifetime Data" (Wiley, New York, 1982) p. 71.

Received 14 March
and accepted 28 July 1988